DNA Damage Signaling in Hematopoietic Cells: A Role for Mre11 Complex Repair of Topoisomerase Lesions

Monica Morales,[1] Yan Liu,[2] Evagelia C. Laiakis,[3] William F. Morgan,[3,4] Stephen D. Nimer,[2] and John H.J. Petrini[1]

[1]Molecular Biology Program, Sloan-Kettering Institute, Memorial Sloan-Kettering Cancer Center and Cornell University Graduate School of Medical Sciences; [2]Molecular Pharmacology and Chemistry Program, Sloan-Kettering Institute, Memorial Sloan-Kettering Cancer Center, New York, New York; and [3]Radiation Oncology Research Laboratory and [4]Marlene and Stewart Greenebaum Cancer Center, University of Maryland School of Medicine, Baltimore, Maryland

Abstract

The Mre11 complex promotes DNA double-strand break repair and regulates DNA damage signaling via activation of the ataxia-telangiectasia mutated (ATM) kinase. The hypermorphic *Rad50*^{S} allele encodes a variant of Rad50, a member of the Mre11 complex. Cells expressing *Rad50*^{S} experience constitutive ATM activation, which leads to precipitous apoptotic attrition in hematopoietic cells. In this study, we show that ATM activation by the *Rad50S*-containing Mre11 complex enhances the proliferation of LSK cells, a population consisting of hematopoietic stem cells and multipotent progenitor cells. In *Rad50*$^{S/S}$ mice, enhanced LSK proliferation triggers apoptotic attrition. This phenotype is mitigated when *Rad50*$^{S/S}$ is combined with mutations that alter either LSK cell quiescence (myeloid elf-1–like factor/ELF4–deficient mice) or hematopoietic differentiation (p21- and p27-deficient mice), indicating that the LSK population is a primary target of *Rad50*^{S} pathology. We show that cells from *Rad50*$^{S/S}$ mice are hypersensitive to camptothecin, a topoisomerase I inhibitor that causes DNA damage primarily during DNA replication. On this basis, we propose that apoptotic attrition of *Rad50*$^{S/S}$ hematopoietic cells results from enhanced proliferation in the context of topoisomerase-associated DNA damage. Impairment of apoptosis in *Rad50*$^{S/S}$ mice promotes hematopoietic malignancy, suggesting that primitive hematopoietic cells serve as a reservoir of potentially oncogenic lesions in *Rad50*$^{S/S}$ mice. These data provide compelling evidence that the Mre11 complex plays a role in the metabolism of topoisomerase lesions in mammals, and further suggest that such lesions can accumulate in primitive hematopoietic cells and confer significant oncogenic potential. [Cancer Res 2008;68(7):2186–93]

Introduction

The Mre11 complex, consisting of Mre11, Rad50, and Nbs1, plays a pivotal role in the DNA damage response, mediating both ataxia-telangiectasia mutated (ATM)–dependent DNA damage signaling and recombinational DNA repair (1). The human chromosome fragility syndromes Nijmegen breakage syndrome and the ataxia-telangiectasia–like disorder (ATLD) result from hypomorphic *Nbs1* and *Mre11* alleles, respectively (2, 3). Cells from mice modeling those disorders exhibit defects in ATM-dependent cell cycle checkpoint functions, as well as hypersensitivity to clastogenic agents such as ionizing radiation. Conversely, mice expressing the *Rad50*^{S} mutation (*Rad50*^{K22M}) are hypermorphic for ATM-dependent signaling and constitutively exhibit indices of genotoxic stress (4–6).

Although the cellular phenotypes of the *Rad50*$^{S/S}$ mutants are mild, the *Rad50*^{S} mutation exerts a profound effect at the organismal level. By 4 weeks of age, the bone marrow of *Rad50*$^{S/S}$ mice is completely devoid of hematopoietic cells, and by 2 months of age most *Rad50*$^{S/S}$ mice die of anemia. Bone marrow reconstitution experiments suggest that this decrement in hematopoietic cellularity results from apoptotic attrition of primitive hematopoietic cells, including the hematopoietic stem cell (HSC) pool. The apoptotic attrition observed is dependent on the DNA damage response pathway governed by the Mre11 complex and ATM (5).

No sensitivity to ionizing radiation, UV radiation, hydroxyurea, or mitomycin C was observed in *Rad50*$^{S/S}$ cells, and ionizing radiation treatment of *Rad50*$^{S/S}$ cells did not result in increased chromosomal aberrations (4, 6). These findings are inconsistent with the interpretation that chronic ATM activation in *Rad50*$^{S/S}$ cells reflected a DNA repair defect. However, in addition to its role in recombinational DNA repair, the Mre11 complex has been implicated in the removal of topoisomerase lesions in several organisms, and the possibility that the metabolism of such lesions is impaired by the *Rad50*^{S} mutation is addressed in this study.

Recent data support the existence of an endonucleolytic DNA repair pathway for the removal of topoisomerase II (Topo II) from DNA ends (7). The cellular nuclease(s) acting in the presumptive Topo II removal pathway are not known. However, the available evidence suggests that the Mre11 nuclease is a likely candidate. For example, Spo11 is liberated from meiotic double-strand break ends covalently bound to short oligonucleotides. The production of this species is blocked in Mre11 nuclease–dead mutants as well as *rad50S* strains. In addition, gp46/gp47 (the Mre11 complex in bacteriophage T4) is required for the nucleolytic removal of covalently attached Topo II in that organism (8–10), and the removal of the terminal protein of adenovirus seems to be blocked by Mre11 depletion in human cells (11). The *S. cerevisiae* Mre11 complex has also been implicated in the repair of topoisomerase I (Topo I) lesions. Rad50 and Mre11 deficiency confers sensitivity to the Topo I inhibitor camptothecin. Reminiscent of Spo11 removal, camptothecin sensitivity is also seen in Mre11 nuclease–dead and *Rad50*$^{S/S}$ mutants, suggesting a role for the Mre11 nuclease in the removal of covalently bound Topo I complexes (12–14).

In this study, we show that precipitous apoptotic loss of hematopoietic cells in *Rad50*$^{S/S}$ mice is due to an intrinsic effect

Note: Supplementary data for this article are available at Cancer Research Online (http://cancerres.aacrjournals.org/).

Requests for reprints: John H.J. Petrini, Laboratory of Chromosome Biology, Memorial Sloan-Kettering Cancer Center, RRL 901C, Box 474, 1275 York Avenue, New York, NY 10021. Phone: 212-639-2927; Fax: 646-422-2062; E-mail: petrinij@mskcc.org.

doi:10.1158/0008-5472.CAN-07-2355

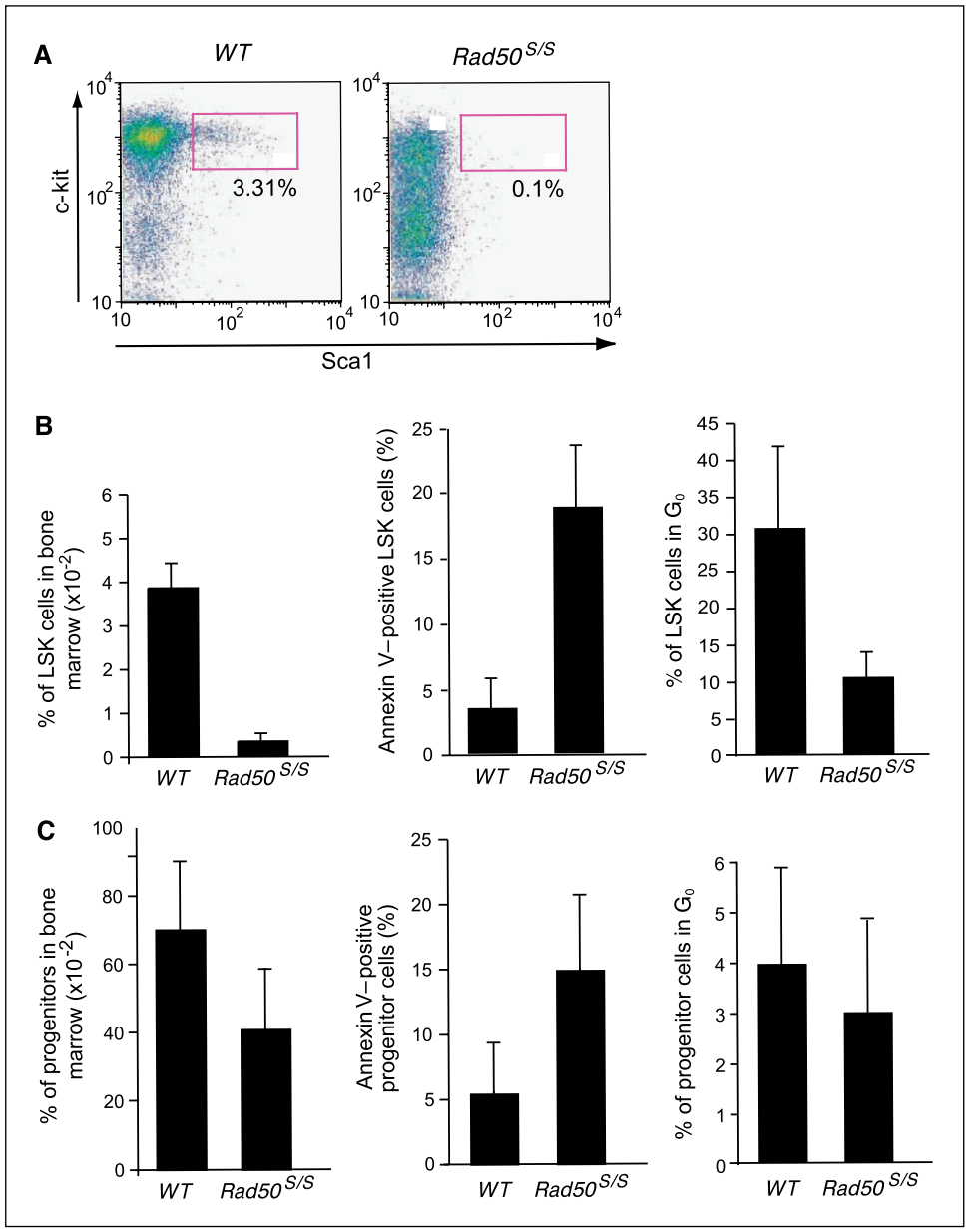

Figure 1. Decreased numbers of LSK and progenitor cells correlate with increased cycling and apoptosis in *Rad50*$^{S/S}$ mice. *A,* representative pseudocolor plots of Lin$^-$ gated cells from 2-week-old *WT* and *Rad50*$^{S/S}$ mice. *B,* decreased LSK frequency, with increased LSK proliferation and apoptosis in *Rad50*$^{S/S}$ mice. *Left,* the percentage of LSK cells from six *WT* and six *Rad50*$^{S/S}$ 2-week-old mice is plotted. $P = 0.004$. *Middle,* percentage of Annexin V–positive LSK cells from the mice depicted on the left. $P = 0.004$. *Right,* percentage of LSK cells that are quiescent (i.e., Ki-67 and Hoechst double-negative) from the mice depicted on the left. $P = 0.004$. *C,* decreased hematopoietic progenitor cell number and apoptosis in *Rad50*$^{S/S}$ mice. *Left,* the percentage of Lin$^-$ Sca-1$^-$ c-kit$^+$ cells from six *WT* and six *Rad50*$^{S/S}$ 2-week-old mice is plotted. $P = 0.037$. *Middle,* percentage of Annexin V–positive Lin$^-$ Sca-1$^-$ c-kit$^+$ cells from the mice depicted on the left. $P = 0.006$. *Right,* percentage of Ki-67 and Hoechst double-negative Lin$^-$ Sca-1$^-$ c-kit$^+$ cells from the mice depicted on the left. $P = 0.34$.

on primitive hematopoietic cells [lineage-negative, Sca-1$^+$, c-kit$^+$ (LSK cells hereafter)]. The hematopoietic attrition is mitigated in genetic contexts that alter LSK cell quiescence or inhibit differentiation, which suggests that the HSC is the primary cell type affected. Activation of the DNA damage response by the *Rad50*^{S} allele causes enhanced proliferation of the LSK pool, which correlates with the induction of apoptosis. When apoptosis is abrogated, LSK cells remain proliferative, suggesting that the *Rad50*^{S} mutation and, by extension, the ATM-dependent DNA damage response reduce quiescence of primitive hematopoietic cells. Further, we present evidence that the repair of topoisomerase lesions is impaired in *Rad50*$^{S/S}$ cells, supporting the view that the Mre11 complex participates in the repair of these lesions *in vivo*. This repair pathway is significant for tumor suppression, as indicated by the fact that apoptotically compromised *Rad50*$^{S/S}$ mice present with myriad hematologic malignancies.

Materials and Methods

Mice derivation and genotyping. *Rad50*$^{S/S}$, *Mef*$^{-/-}$, *p21*$^{-/-}$, *p27*$^{-/-}$, *Atm*$^{-/-}$, *Mre11*$^{ATLD1/ATLD1}$, *Chk2*$^{-/-}$, *Rad50*$^{S/S}$ *Atm*$^{-/-}$, *Rad50*$^{S/S}$ *Mre11*$^{ATLD1/ATLD1}$, and *Rad50*$^{S/S}$ *Chk2*$^{-/-}$ survival and genotyping have been described (3, 5, 6, 15–19). *Rad50*$^{S/S}$ *Mef*$^{-/-}$, *Rad50*$^{S/S}$ *p21*$^{-/-}$, and *Rad50*$^{S/S}$ *p27*$^{-/-}$ double mutant animals were generated in this study. All mice were derived at Memorial Sloan Kettering Cancer Center and maintained on mixed 129/SvEv and C57BL/6 background. All experiments involving animals conform to Institutional Animal Care and Use Committee institutional and national standards.

Survival analyses and statistical significance. Kaplan-Meier survival curves were made with Prism 4 (GraphPad Software). Statistical significance for all studies was determined by a two-sided Wilcoxon rank sum test using Mstat software (Norman Drinkwater, McArdle Laboratory for Cancer Research).

Hematopoietic cell preparation and analysis. Single-cell suspensions from the bone marrow were depleted of RBC by hypotonic lysis and maintained in PBS. Labeled antibodies specific for B220 (phycoerythrin),

IgM (FITC), CD43 (FITC), Cd11b (phycoerythrin), Gr-1 (FITC), c-kit (allophycocyanin), Sca-1 (phycoerythrin), Annexin V (FITC), biotinylated mouse lineage panel, and streptavidin-allophycocyanin-Cy7 were from BD Biosciences PharMingen. Ki-67 (FITC) antibody was from Vector Lab, Inc., and Hoechst 33342 from Molecular Probes. Dead cells were excluded by propidium iodide staining. The number of pro-B cells was equal to the number of B220 CD43 double-positive bone marrow cells; the number of pre-B cells was the number of B220-positive, CD43-negative, IgM-negative cells; the number of Immature B cells was the number of B220 IgM double-positive cells; and the number of myeloid cells was the number of Gr-1 Cd11b double-positive cells. The number of LSK cells was the number of lineage-negative, c-kit–positive, Sca-1–positive cells, and the number of progenitors was the number of lineage-negative, Sca-1–negative, c-kit–positive cells. Fluorescence-activated cell sorting (FACS) analyses were done on FACSCalibur Instruments (Becton Dickinson).

Colony-forming cell assay. Clonogenic progenitors were determined in methylcellulose medium (MethoCult GF M3434, Stem Cell Technologies) using 2×10^4 bone marrow mononuclear cells per well (six-well plate). Colonies were scored after 10 d of incubation and expressed as number of colony-forming cells (CFC) per total bone marrow (two femurs and two tibias).

Cell derivation and culture. Murine embryonic fibroblasts (MEF) and murine ear fibroblasts were generated and cultured as described (6). SV40 immortalization was achieved as described (6).

Cellular assays. Sensitivity to clastogens was assessed by colony formation assays as described (3) and the surviving fraction was determined after 9 d in culture. Metaphase preparations, conventional karyotypic analyses, and telomere fluorescence *in situ* hybridization (FISH) analyses were done as previously described (6). For sister chromatid exchange (SCE) analyses, cells were grown for 40 h in 30 μg/mL bromodeoxyuridine, and camptothecin treatments were done as for the conventional analyses. Metaphases were dropped on slides and aged overnight. Slides were rinsed for 10 min in 2× SSC (0.3 mol/L NaCl and 0.03 mol/L sodium citrate, pH 7.0) and then soaked for 20 min in 2.5 mg/mL Hoechst (Sigma B-1155) made in 2× SSC. After rinsing in H_2O, a few drops of 2× SSC and a glass coverslip were added. Slides were irradiated for 4 min at 55°C under a UV lamp and stained in 5% Giemsa for 40 min before analysis. All analyses were carried out on blinded samples.

Results and Discussion

We have previously shown that the *Rad50*^{S} allele and, by extension, the Mre11 complex induce apoptosis via the chronic activation of the DNA damage response pathway governed by the Mre11 complex, ATM, p53, and Chk2 (5). As a consequence, *Rad50*$^{S/S}$ mice exhibit fatal anemia and bone marrow aplasia associated with HSC depletion (6). Two explanations for the bone marrow failure observed have been considered: First, the widespread hematopoietic attrition in *Rad50*$^{S/S}$ mice may result in homeostatic stress and lead to precipitous exhaustion of the HSC pool (6). An alternative and nonexclusive interpretation is that chronic DNA damage signaling by the *Rad50*^{S} allele exerts an intrinsic effect on the HSC compartment, leading to its depletion by apoptosis.

To address this issue, we examined the hematopoietic compartment of 2-week-old *Rad50*$^{S/S}$ mice. This early time point was necessary because most *Rad50*$^{S/S}$ mice become severely anemic by 4 weeks of age and moribund by 6 to 8 weeks (6). This outcome is intrinsic to *Rad50*$^{S/S}$ hematopoietic cells (i.e., not attributable to

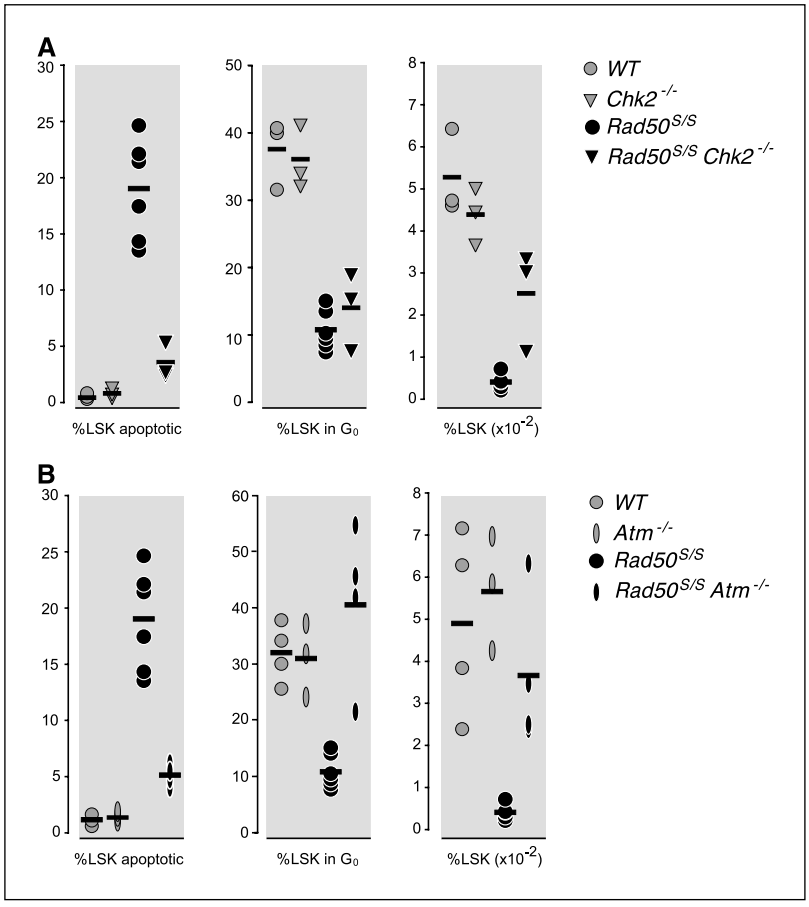

Figure 2. *A,* percentages of Annexin V–positive (*left*) and Ki-67 and Hoechst double-negative (*middle*) LSK cells and total number of LSK cells (*right*) in the bone marrow of *WT, Chk2*$^{-/-}$, *Rad50*$^{S/S}$, and *Rad50*$^{S/S}$ *Chk2*$^{-/-}$ mice. *B,* percentages of Annexin V–positive (*left*) and Ki-67 and Hoechst double-negative (*middle*) LSK cells and total number of LSK cells (*right*) in the bone marrow of *WT, Atm*$^{-/-}$, *Rad50*$^{S/S}$, and *Rad50*$^{S/S}$ *Atm*$^{-/-}$ mice.

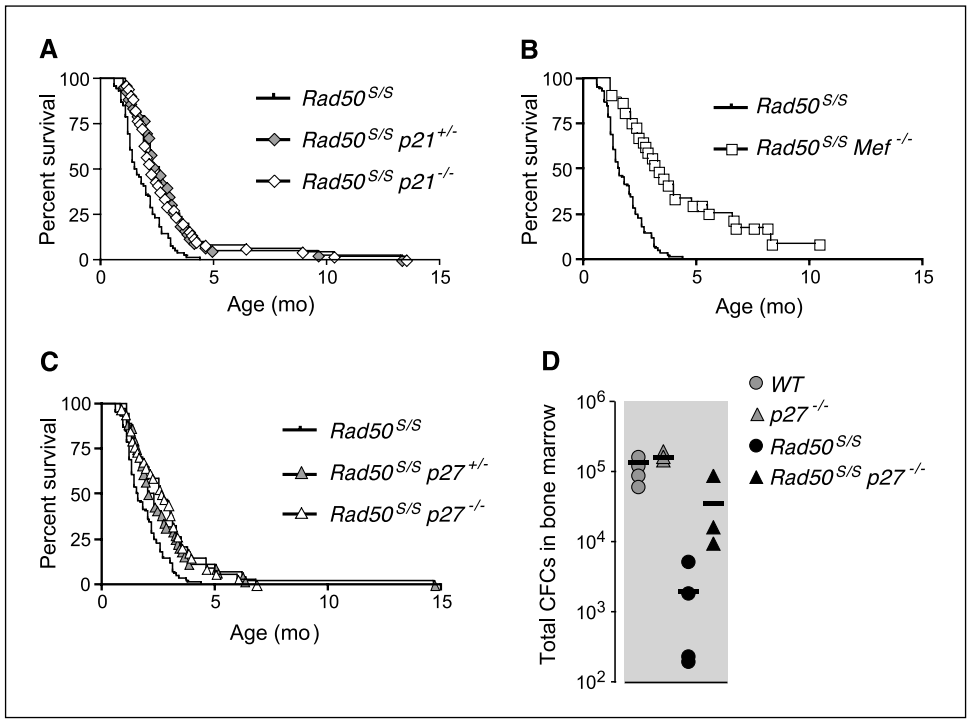

Figure 3. Enhanced survival of *Rad50*$^{S/S}$ mice by p21, Mef, or p27 deficiencies. *A,* Kaplan-Meier survival curves of *Rad50*$^{S/S}$ (n = 84), *Rad50*$^{S/S}$ *p21*$^{+/-}$ (n = 43), and *Rad50*$^{S/S}$ *p21*$^{-/-}$ (n = 51) mice. *B,* Kaplan-Meier survival curves of *Rad50*$^{S/S}$ (n = 84) and *Rad50*$^{S/S}$ *Mef*$^{-/-}$ (n = 27) mice. *C,* Kaplan-Meier survival curves of *Rad50*$^{S/S}$ (n = 84), *Rad50*$^{S/S}$ *p27*$^{+/-}$ (n = 44), and *Rad50*$^{S/S}$ *p27*$^{-/-}$ (n = 34) mice. *D,* hematopoietic progenitor numbers were quantified by the CFC assay using 20,000 bone marrow mononuclear cells from 4-week-old mice.

stromal defects), as *Rad50*$^{S/S}$ fetal liver-derived HSC do not support hematopoietic differentiation in *WT* mice, even when transplanted in the presence of *WT* fetal liver cells (6). Hematopoietic progenitor cells and mature hematopoietic cells are also subject to apoptotic attrition in *Rad50*$^{S/S}$ mice (5, 6). However, because LSK cells are significantly reduced (>90% at 2 weeks of age) when progenitor (Lin^-, c-kit^+, Sca-1^-) cells from mice of the same age show only a 2-fold reduction in frequency (Fig. 1*C*), we focused on the LSK cells for this study.

First, we assessed by flow cytometry the frequency of lineage-negative, Sca-1–positive, and c-kit–positive (LSK) cells, a population shown to be enriched in HSCs and multipotent progenitors (20–26). In *WT* animals, this population confers both short-term and long-term hematopoietic reconstitution of irradiated recipients. Although the bone marrow cellularity of 2-week-old *Rad50*$^{S/S}$ mice remained 80% to 90% of that of *WT* littermates (data not shown), the LSK frequency of *Rad50*$^{S/S}$ was reduced to 8% of *WT* cells (Fig. 1*A* and *B* and Supplementary Fig. S1).

These analyses also revealed that *Rad50*$^{S/S}$ LSK cells exhibited markedly increased levels of apoptotic cells; only 3.5% of LSK cells in *WT* bone marrow stained positive for Annexin V, whereas 18.8% of *Rad50*$^{S/S}$ LSK cells were positive (Fig. 1*B* and Supplementary Fig. S2). This result shows that the increased apoptosis is intrinsic to the *Rad50*$^{S/S}$ LSK compartment. In addition, an aberrantly large fraction of *Rad50*$^{S/S}$ LSK cells were in cycle, as evidenced by elevated Ki-67 and Hoechst double staining in the *Rad50*$^{S/S}$ LSK population (Fig. 1*B* and Supplementary Fig. S3). In *WT* mice 30.6% of LSK cells are quiescent (i.e., Ki-67 and Hoechst double negative), compared with 10.5% in *Rad50*$^{S/S}$ LSK.

The reduction in *Rad50*$^{S/S}$ LSK quiescence was observed at 2 weeks of age, before significant depletion of hematopoietic bone marrow cells. This suggested that increased LSK proliferation in *Rad50*$^{S/S}$ was not a homeostatic response to depletion of more mature hematopoietic cells in the bone marrow. We tested this interpretation by crossing *Rad50*$^{S/S}$ to *Chk2*$^{-/-}$, which blocks apoptosis of hematopoietic cells in *Rad50*$^{S/S}$ mice (5). We reasoned that impaired apoptosis in Chk2 deficiency would eliminate homeostatic pressure on the LSK population and restore quiescence to normal levels. As expected, the apoptotic fraction of *Rad50*$^{S/S}$ *Chk2*$^{-/-}$ LSK cells was reduced to *WT* levels (Fig. 2*A*); however, the quiescent fraction of *Rad50*$^{S/S}$ *Chk2*$^{-/-}$ cells was unchanged. In *Rad50*$^{S/S}$ *Chk2*$^{-/-}$ LSK, 14.4% were Ki-67 and Hoechst double negative (Fig. 2*A*), a fraction similar to the 10.5% observed in *Rad50*$^{S/S}$ LSK. The fraction of Ki-67–positive cells returned to *WT* levels in both *Rad50*$^{S/S}$ *Atm*$^{+/-}$ and *Rad50*$^{S/S}$ *Atm*$^{-/-}$ mice (Fig. 2*B* and data not shown). These results strongly support the view that reduced LSK cell quiescence and enhanced apoptosis are cell-intrinsic effects of the Mre11 complex-ATM signaling pathway.

To delineate the relative effect of *Rad50*$^{S/S}$ on LSK cells versus their progeny, the number or cycling characteristics of LSK cells were manipulated genetically. The cyclin-dependent kinase inhibitors p21 and p27 interdict hematopoietic development primarily in HSCs and hematopoietic progenitor cells, respectively; HSC numbers seem to be elevated by p21 deficiency (27) whereas progenitor pools are expanded by p27 deficiency (28). LSK quiescence was altered by crossing *Rad50*$^{S/S}$ to mice deficient for the transcription factor myeloid elf-1–like factor (Mef/ELF4). Mef promotes the entry of primitive hematopoietic cells into cycle, and in *Mef*$^{-/-}$ mice quiescence is markedly enhanced (15). Whereas both *p21*$^{-/-}$ and *Mef*$^{-/-}$ mice exhibit increased numbers of HSC, only Mef seems to exert an effect on quiescence (Fig. 4*A*; refs. 27, 29).

Deficiency of Mef, p21, or p27 increased the survival of *Rad50*$^{S/S}$ mice ($P < 10^{-4}$). Whereas only 1.2% of *Rad50*$^{S/S}$ mice survived past 4 months of age, 15.7% of *Rad50*$^{S/S}$ *p21*$^{-/-}$ double mutants and 29.4% of *Rad50*$^{S/S}$ *Mef*$^{-/-}$ animals survived beyond 4 months (Fig. 3*A* and *B*). p27 deficiency increased *Rad50*$^{S/S}$ survival to a similar extent as p21 deficiency (Fig. 3*C*; $P < 10^{-4}$).

Despite the enhanced survival of *Rad50*$^{S/S}$ double mutant animals, the *Rad50*^{S}-dependent attrition of committed lymphoid and myeloid precursors was not mitigated in *p21*$^{-/-}$ and *Mef*$^{-/-}$ (Supplementary Fig. S4*A* and *B*). However, p27 deficiency mitigated *Rad50*$^{S/S}$ hematopoietic attrition; *Rad50*$^{S/S}$ *p27*$^{-/-}$ mice exhibited 3.7-fold the number of pro-B cells and 2.5-fold the number of immature B cells present in *Rad50*$^{S/S}$ mice (Supplementary Fig. S4*C*). No effect on pre-B or myeloid cells was observed (Supplementary Fig. S4*C*). These data indicate that mitigation of the *Rad50*$^{S/S}$ phenotype can be achieved via expansion of either the HSC pool or the precursor pool.

This interpretation is supported by direct analysis of hematopoietic progenitor cell numbers in 4-week-old *Rad50*$^{S/S}$, *p27*$^{-/-}$, and *Rad50*$^{S/S}$ *p27*$^{-/-}$ mice using methylcellulose CFC assays (27, 28). As previously described (28), *p27*$^{-/-}$ mice exhibited a 2-fold increase in progenitors over *WT* (Fig. 3*D*). Whereas *Rad50*$^{S/S}$ mice showed a 50-fold decrease in progenitor cell numbers, CFCs were within 5-fold of *WT* in *Rad50*$^{S/S}$ *p27*$^{-/-}$ (Fig. 3*D*). These data indicate that some rescue of the *Rad50*$^{S/S}$ phenotype in *Rad50*$^{S/S}$ *p27*$^{-/-}$ animals is associated with expansion of the progenitor pool.

Conversely, LSK cell frequencies were elevated in both p21- and Mef-deficient *Rad50*$^{S/S}$ mice when compared with *Rad50*$^{S/S}$, and the extent of the LSK increase correlated with the enhancement in survival (Fig. 4*A* and Supplementary Fig. S1). Whereas *Rad50*$^{S/S}$ *p21*$^{-/-}$ had twice as many LSK cells as *Rad50*$^{S/S}$ at 2 weeks of age, age, *Rad50*$^{S/S}$ *Mef*$^{-/-}$ showed a 4.3-fold increase (to 36% of that of *WT* *WT* animals; Fig. 4*A* and Supplementary Fig. S1). A switch from fetal to adult hematopoiesis seems to occur at 4 weeks of age. Previous analyses of *Mef*$^{-/-}$ C57BL/6 or *p21*$^{-/-}$ 129/Sv were done on 8- to 12-week-old mice (15, 27) when hematopoiesis is of the adult type, a time frame inaccessible in *Rad50*$^{S/S}$ mice. Thus, age at the time of analysis of LSK cells, necessitated by the *Rad50*$^{S/S}$ phenotype, may account for differences between the data presented here and those previously reported for *Mef*$^{-/-}$ (15) and *p21*$^{-/-}$. Moreover, the analysis of *p21*$^{-/-}$ assessed HSC frequency by colony assay (cobblestone area–forming cell assays) and not by FACS (27).

Having established that increased numbers of LSK cells were correlated with increased survival in *Rad50*$^{S/S}$ *p21*$^{-/-}$ and *Rad50*$^{S/S}$ *Mef*$^{-/-}$ mice, we examined the effects on the quiescence and apoptotic phenotypes of *Rad50*$^{S/S}$. The quiescence of the LSK population of *Rad50*$^{S/S}$ *Mef*$^{-/-}$ animals was increased compared with that of *Rad50*$^{S/S}$ mice (21% versus 10.5%, respectively; Fig. 4*B* and Supplementary Fig. S3). In contrast, p21 deficiency had no effect on LSK quiescence. In *Rad50*$^{S/S}$ *p21*$^{-/-}$ LSK, 91.4% were cycling cells, which was similar to the 89.5% cycling of LSK cells in *Rad50*$^{S/S}$ mice (Fig. 4*B* and Supplementary Fig. S3). The effects of p21 and Mef-deficiency on LSK cell quiescence were correlated with the levels of apoptosis. Whereas 5% of *WT*, *p21*$^{-/-}$, and *Mef*$^{-/-}$ LSK stained positive for Annexin V, 18.8% of *Rad50*$^{S/S}$ and 19.25% of *Rad50*$^{S/S}$ *p21*$^{-/-}$ LSK cells were apoptotic (Fig. 4*C* and Supplementary Fig. S2). This was reduced to only 4.1% *Rad50*$^{S/S}$ *Mef*$^{-/-}$ LSK cells. These results suggest that apoptosis of *Rad50*$^{S/S}$ LSK is dependent on their entry into the cell cycle. Supporting this view, 2 days of treatment with granulocyte colony-stimulating factor (G-CSF), given to induce HSC entry into cycle (30), obliterated the bone marrow LSK pool in 2-week-old *Rad50*$^{S/S}$ mice (Fig. 4*D*). Furthermore, whereas G-CSF treatment did not appreciably alter the frequency or the apoptosis of LSK cells in *WT* and *Mef*$^{-/-}$ mice, the LSK pool was markedly reduced in *Rad50*$^{S/S}$ *Mef*$^{-/-}$ double mutants, from 0.014% of total bone marrow cells before G-CSF–induced cycling

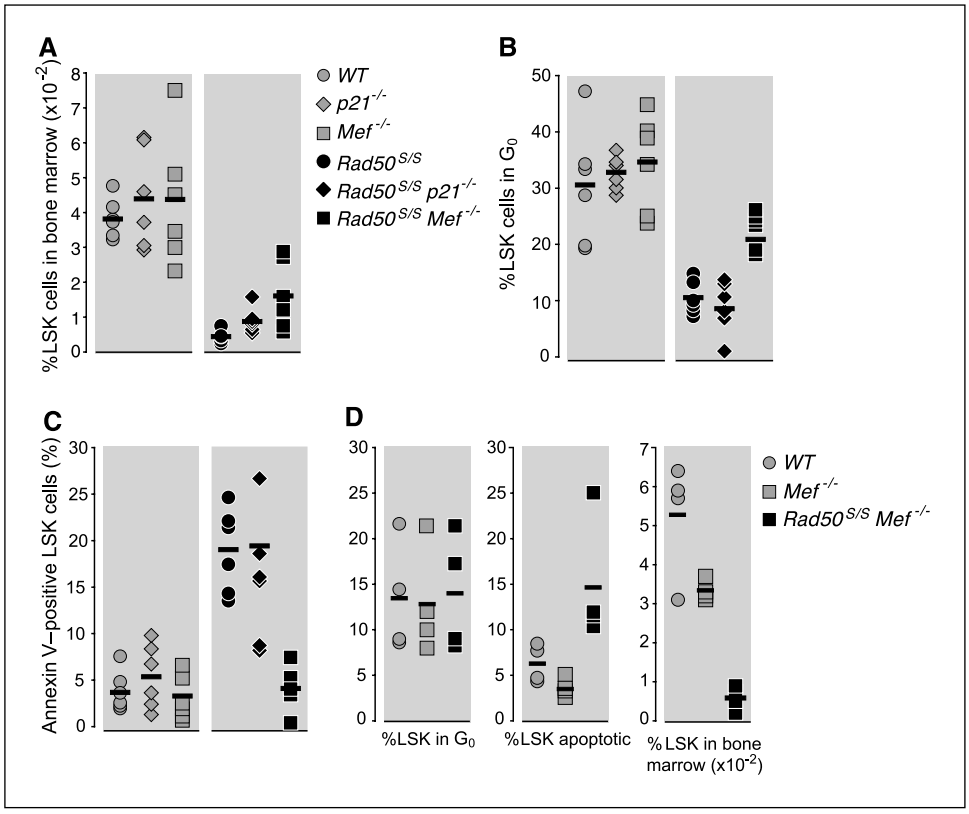

Figure 4. Maintenance of LSK quiescence abrogates LSK apoptosis in *Rad50*$^{S/S}$ mice. *A,* the percentage of Lin^{-} Sca-1^{+} c-kit^{+} (LSK) cells from 2-week-old *WT*, *Mef*$^{-/-}$, *p21*$^{-/-}$, *Rad50*$^{S/S}$, *Rad50*$^{S/S}$ *Mef*$^{-/-}$, and *Rad50*$^{S/S}$ *p21*$^{-/-}$ mice is plotted ($n = 6$). $P = 0.02$, *Rad50*$^{S/S}$ versus *Rad50*$^{S/S}$ *p21*$^{-/-}$; $P = 0.01$, *Rad50*$^{S/S}$ versus *Rad50*$^{S/S}$ *Mef*$^{-/-}$. *B,* percentage of Ki-67 and Hoechst double-negative LSK cells from the mice depicted in *A*. Symbols as in *A*. $P = 0.631$, *Rad50*$^{S/S}$ versus *Rad50*$^{S/S}$ *p21*$^{-/-}$; $P = 0.037$, *Rad50*$^{S/S}$ and *Rad50*$^{S/S}$ *Mef*$^{-/-}$. *C,* percentage of Annexin V–positive LSK cells from the mice depicted in *A*. Symbols as in *A*. $P = 0.423$, *Rad50*$^{S/S}$ versus *Rad50*$^{S/S}$ *p21*$^{-/-}$; $P = 0.004$, *Rad50*$^{S/S}$ versus *Rad50*$^{S/S}$ *Mef*$^{-/-}$. *D, WT, Mef*$^{-/-}$, *Rad50*$^{S/S}$, and *Rad50*$^{S/S}$ *Mef*$^{-/-}$ LSK were pushed into cycle with 2-d sequential injections of 250 μg/kg G-CSF. On day 3, the percentage of LSK cells in bone marrow was measured ($n = 4$; *left*). *Middle* and *right,* the percentages of Annexin V–positive or Ki-67 and Hoechst double-negative LSK cells are plotted, respectively.

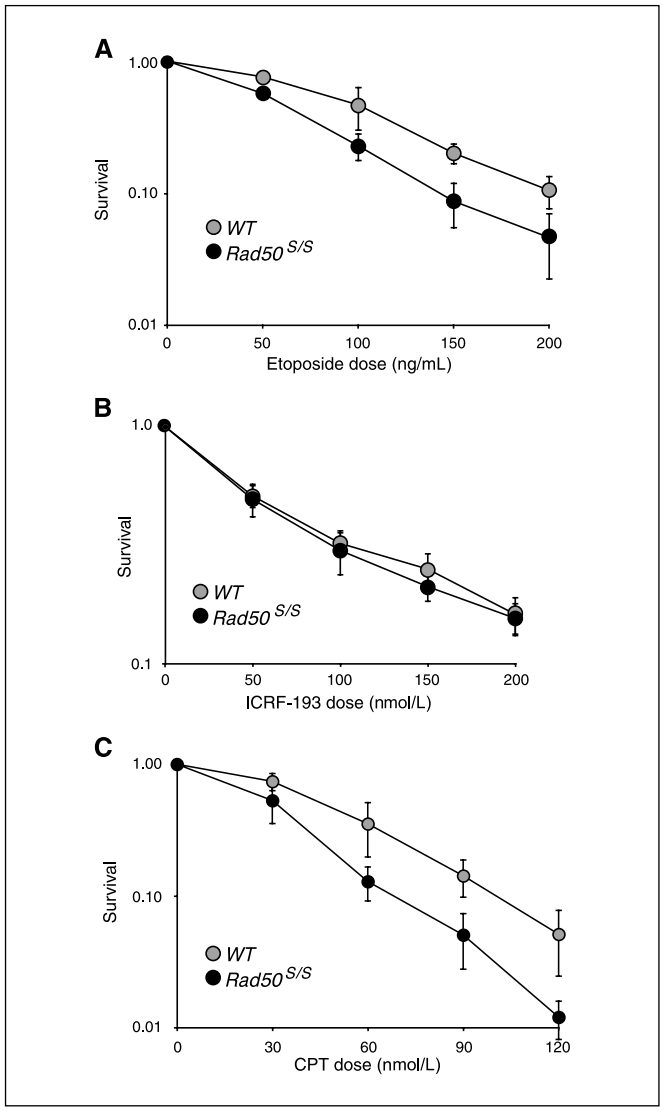

Figure 5. *Rad50*$^{S/S}$ cells are hypersensitive to etoposide and camptothecin. Sensitivity determined by colony-forming assay. Each graph is a compilation of three experiments from different cultures in which cells were plated in triplicate at each dose. *A,* surviving fractions of *WT* and *Rad50*$^{S/S}$ SV40-transformed MEFs after a 24-h treatment with various doses of etoposide. *B,* surviving fractions of *WT* and *Rad50*$^{S/S}$ SV40-transformed MEFs after a 24-h treatment with various doses of ICRF-193. *C,* surviving fractions of *WT* and *Rad50*$^{S/S}$ SV40-transformed MEFs after a 24-h treatment with various doses of camptothecin (*CPT*).

(Fig. 4*A*) to 0.006% after G-CSF treatment (Fig. 4*D*). This LSK cell depletion correlated with increased levels of apoptosis (Fig. 4*D*). These data are consistent with the view that apoptotic attrition of *Rad50*$^{S/S}$ LSK cells is driven by cell cycle entry.

A striking feature of the *Rad50*$^{S/S}$ double mutants examined was the frequent occurrence of hematopoietic malignancies: 37.5% of *Rad50*$^{S/S}$ *p21*$^{-/-}$, 30% of *Rad50*$^{S/S}$ *Mef*$^{-/-}$, and 35.7% of *Rad50*$^{S/S}$ *p27*$^{-/-}$ animals developed tumors (Supplementary Table S1), whereas none were observed in *Mef*$^{-/-}$, *p21*$^{-/-}$ or *p27*$^{-/-}$ mice, and in *Rad50*$^{S/S}$ mice, tumors are exceedingly rare (15–17, 31, 32). Malignancy was restricted to the hematopoietic compartments, with both myeloid and lymphoid neoplasms occurring (data not shown). A similar result was observed previously in *Rad50*$^{S/S}$ mice that also harbor mutations that attenuate ATM-dependent apoptosis: 12 of 14 *Rad50*$^{S/S}$ *Mre11*$^{ATLD1/ATLD1}$ and 17 of 22 *Rad50*$^{S/S}$ *Chk2*$^{-/-}$ mice died with malignancies (ref. 5; Supplementary Table S1), whereas no malignancy was seen in *Mre11*$^{ATLD1/ATLD1}$ mice (3) or *Chk2*$^{-/-}$ mice (19).

These results indicate that the *Rad50*^{S} allele predisposes to malignancy to a greater extent than previously observed, and suggest the possibility that oncogenic DNA damage accumulates in *Rad50*$^{S/S}$ cells. We previously proposed that the metabolism of topoisomerase lesions may be impaired in *Rad50*$^{S/S}$ cells (5). This proposal was primarily based on the fact that removal of the Topo II–like molecule Spo11 from double-strand break ends formed in meiosis is blocked in *S. cerevisiae Rad50*^{S} mutants (7). Because an aberrantly large fraction of *Rad50*$^{S/S}$ LSK cells are cycling, it is plausible that the attrition of primitive hematopoietic cells and the predisposition to hematopoietic malignancy result from defective resolution of topoisomerase cleavage complexes.

The ability of *Rad50*$^{S/S}$ cells to metabolize topoisomerase lesions was tested by treatment with camptothecin and etoposide, which stabilize covalent Topo I and Topo II covalent complexes, respectively (33, 34). Presumably because the baseline level of apoptosis was high, we were unable to detect increased apoptosis in *Rad50*$^{S/S}$ hematopoietic cells on camptothecin treatment (data not shown). The effects of these drugs on MEFs and ear fibroblasts were examined. *Rad50*$^{S/S}$ cells were slightly more sensitive to etoposide than *WT* cells, as measured by colony-forming ability after a 24-hour treatment (Fig. 5*A*). This subtle difference seems to reflect a defect in processing Topo II lesions, as *Rad50*$^{S/S}$ were not sensitive to ICRF-193 (Fig. 5*B*), a catalytic inhibitor that blocks the formation of the Topo II cleavage complex (35). *Rad50*$^{S/S}$ cells were markedly more sensitive to camptothecin (Fig. 5*C*). The increased sensitivity was not a consequence of defective cell cycle arrest; both *WT* and *Rad50*$^{S/S}$ cells arrested in S phase and at the G_2 phase of the cell cycle on treatment with camptothecin (data not shown).

Consistent with their relative effects on colony-forming ability, acute exposure of *Rad50*$^{S/S}$ cells to camptothecin, but not etoposide, increased the induction of chromosome aberrations (Fig. 6*A* and Supplementary Fig. S5). Cells were treated briefly (2 hours) with etoposide or camptothecin, and mitotic spreads prepared 4 to 6 hours later. In this way, metaphase cells would have been in S phase during drug treatment. Whereas 79% of *WT* metaphases exhibited no aberrations after a 2-hour treatment with camptothecin, only 59% were free of aberrations in *Rad50*$^{S/S}$ cells (Fig. 6*A*; $P < 10^{-3}$). Moreover, the spectrum of aberrations differed significantly. Of the aberrations present in *WT* cells, 65% were breaks and chromatid fragments, whereas the other 35% were fusions and exchanges (Fig. 6*B*). In contrast, the distribution was reversed in *Rad50*$^{S/S}$ cells, with 64% of aberrations being fusions and exchanges, and 36% breaks and fragments (Fig. 6*B*). Telomere FISH analysis was used to distinguish short-arm exchanges from telomeric fusions (Fig. 6*C*). Eighty percent of the aberrations scored by FISH in *Rad50*$^{S/S}$ cells were short-arm exchanges, whereas only end fusions were present in *WT* cells (Fig. 6*C*).

This spectrum of aberrations suggests that camptothecin-stabilized Topo I cleavage complexes induce recombination in *Rad50*$^{S/S}$. This interpretation predicted that camptothecin treatment of *Rad50*$^{S/S}$ cells would induce increased levels of SCE. This prediction was met, as the SCE frequency induced by camptothecin was enhanced in *Rad50*$^{S/S}$ compared with *WT* cells (1.055 versus 0.559 SCE/chromosome, respectively; Fig. 6*D*). In this context, it is noteworthy that lymphomas arising in *Rad50*$^{S/S}$ *p53*$^{-/-}$ mice exhibited a complex spectrum of nonclonal

chromosomal aberrations (6), consistent with the possibility that increased levels of chromosome rearrangement are induced by the *Rad50*^{S} allele. Collectively, these results indicate that the *Rad50*^{S} mutation impairs the processing of topoisomerase cleavage complexes, and suggest that accumulation of this form of DNA damage in *Rad50*$^{S/S}$ cells markedly predisposes to both apoptosis and malignancy.

This study shows a role for the Mre11 complex in the repair of topoisomerase-associated DNA damage in mammalian cells. In *S. cerevisiae*, this function has been suggested for Topo I lesions by the extreme cytostatic effects of camptothecin in Mre11 complex nuclease–deficient mutants, as well as from genetic interactions with mutations affecting enzymes such as tyrosyl-DNA-phosphodiesterase that participate in the resolution of the Topo I-DNA linkage (36). Evidence for a repair pathway in *S. cerevisiae* and mammals dedicated to the resolution of Topo II lesions has recently emerged (7). The observation of *Rad50*$^{S/S}$ etoposide sensitivity presented here suggests that the Mre11 complex contributes to this pathway (Fig. 5*A*), consistent with the requirement for the Mre11 nuclease for the removal of Spo11 in meiosis.

In addition, we have established that chronic Mre11 complex–dependent DNA damage signaling in *Rad50*$^{S/S}$ mice impairs the quiescence of LSK cells and triggers apoptosis. The effect is cell-intrinsic and does not seem to reflect a homeostatic response to the reduced presence of more mature hematopoietic cells in *Rad50*$^{S/S}$ mice. Hence, the effect of the Mre11 complex-ATM–dependent pathway on HSC cycling starkly contrasts the effect of this pathway in most cells where cycling is suppressed in response to DNA damage rather than enhanced. This effect of the *Rad50*^{S} allele is not restricted to hematopoietic cells because apoptotic loss of spermatogenic cells and gut epithelia with the same genetic dependencies has been observed (5, 6, 37).

This paradoxical outcome may serve to effectively preserve the integrity of primitive hematopoietic components. In this scenario, entry of HSCs experiencing DNA damage into the cell cycle could increase the likelihood that nonmutagenic DNA repair such as homologous recombination will occur. Entry into S phase would provide a sister chromatid for this mode of repair, and thus could not occur in quiescent cells. Entry into the cell cycle may also increase the efficiency with which apoptosis is induced, thereby facilitating the culling of damaged HSCs from the pool. The observed effect of *Rad50*^{S} on HSC quiescence raises the possibility that compounds mimicking the *Rad50*^{S} effect could be used to induce cycling in quiescent cells that carry oncogenic mutations and thus render them more sensitive to cytotoxic chemotherapies.

Finally, we found that p21 and p27 deficiencies promote malignancy in *Rad50*$^{S/S}$ mice to an extent similar to mutations that impair ATM signaling and apoptosis (5). It is unlikely that ATM regulation is affected by loss of p21 or p27. Thus, the tumor-suppressive effects of p21 and p27 are likely to be via their regulation of hematopoietic cell growth and differentiation. However, recent data show that p27 suppresses prostate cancer independently of its effect on cell cycle regulation. It has been proposed that genome stability, as well as apoptosis, may be affected by p27 (38, 39). The tumor outcome in *Rad50*$^{S/S}$ *Mef*$^{-/-}$ is more complex, but is also likely to reflect its influence on differentiation. In ovarian tissues, Mef also functions as an oncogene that drives proliferation when overexpressed or limits

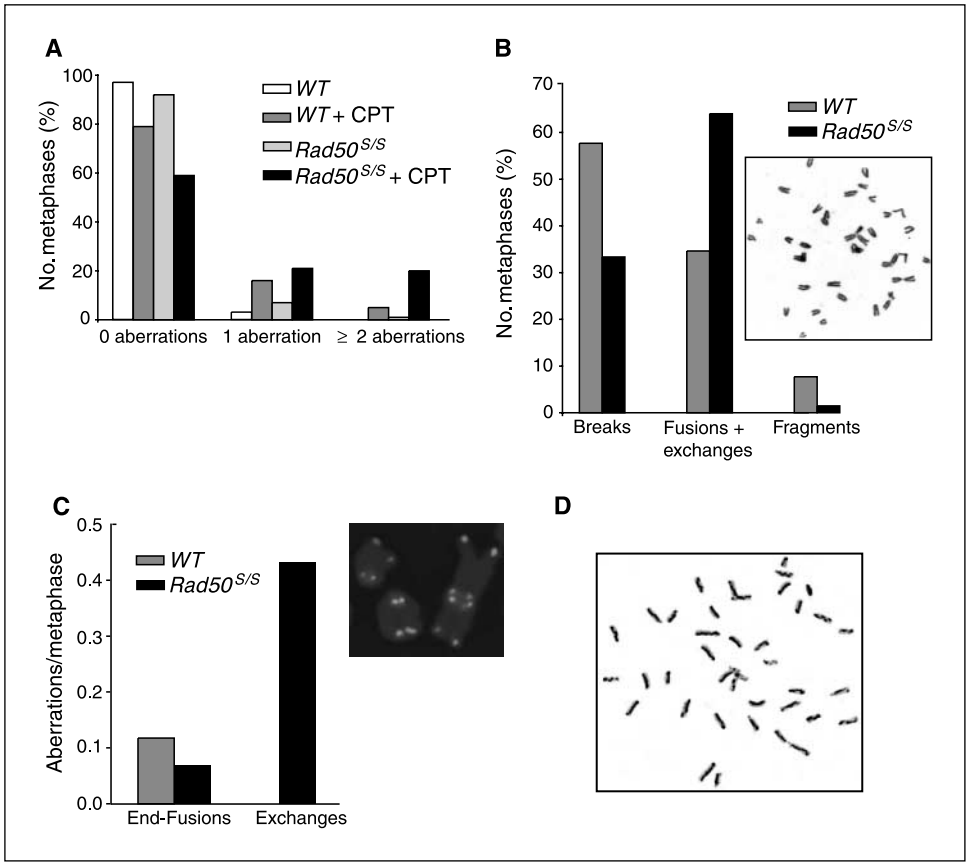

Figure 6. *Rad50*$^{S/S}$ cells show enhanced chromosomal instability in response to camptothecin. Primary ear fibroblasts were treated with 25 nmol/L camptothecin for 2 h. Camptothecin was washed away and cells were allowed to recover for 2.5 h. Then colcemid was added and cells were incubated for an additional 3.5 h before metaphases were prepared. *A,* the percentage of cells with 0, 1, or 2 or more chromosome aberrations is depicted. One hundred metaphases were scored per each genotype and treatment. *B,* the types of aberrations from the camptothecin-treated metaphases scored in *D* are depicted as percentage of the total number of aberrations. *Inset,* a representative metaphase of *Rad50*$^{S/S}$ cells treated with camptothecin. *C,* the graph shows the total numbers of end fusions and exchanges from *WT* and *Rad50*$^{S/S}$ cells treated with camptothecin, as measured by telomere FISH. One hundred metaphases were scored. Mock-treated *WT* and *Rad50*$^{S/S}$ cells were included in the experiment and showed no fusions or exchanges. *Inset,* a representative image of *Rad50*$^{S/S}$ cells treated with camptothecin. Note that 4′,6-diamidino-2-phenylindole was pseudocolored red. *D,* a representative figure of the SCE observed in *Rad50*$^{S/S}$ cells treated with camptothecin. SCE/chromosome: 0.338 in *WT* cells, 0.395 in *Rad50*$^{S/S}$, 0.559 in *WT* treated with camptothecin, and 1.055 in *Rad50*$^{S/S}$ treated with camptothecin.

proliferation when depleted (40). In *Rad50*$^{S/S}$ mice, the effect of Mef deficiency on quiescence rescues the LSK cells from elimination, but as it has not been shown to function as a tumor suppressor, the tumors formed in *Rad50*$^{S/S}$ *Mef*$^{-/-}$ animals are likely to result from *Rad50*^{S}-associated oncogenic mutations. Whether dependent or independent of their effects on cell growth, our data underscore the role of cell cycle regulators (including Mef, p21, and p27) in the suppression of hematopoietic malignancy.

Acknowledgments

Received 6/23/2007; revised 12/4/2007; accepted 1/21/2008.

Grant support: NIH grants GM56888 and GM59413 and the Joel and Joan Smilow Initiative (J.H.J. Petrini), Department of Energy grant DE-FG02-99ER62859 (W.F. Morgan), and NIH grants R01-DK52208 and R01-DK52621 (S.D. Nimer).

The costs of publication of this article were defrayed in part by the payment of page charges. This article must therefore be hereby marked *advertisement* in accordance with 18 U.S.C. Section 1734 solely to indicate this fact.

We thank Andy Koff, Mark Frattini, and the members of our labs for the careful reading of the manuscript, and Daniel Lacorazza for his help with the stem cell assays.

References

1. Stracker TH, Theunissen JW, Morales M, Petrini JH. The Mre11 complex and the metabolism of chromosome breaks: the importance of communicating and holding things together. DNA repair 2004;3:845–54.
2. Williams BR, Mirzoeva OK, Morgan WF, Lin J, Dunnick W, Petrini JH. A murine model of nijmegen breakage syndrome. Curr Biol 2002;12:648–53.
3. Theunissen JW, Kaplan MI, Hunt PA, et al. Checkpoint failure and chromosomal instability without lymphomagenesis in Mre11(ATLD1/ATLD1) mice. Molecular cell 2003;12:1511–23.
4. Usui T, Petrini JH, Morales M. Rad50S alleles of the Mre11 complex: questions answered and questions raised. Exp Cell Res 2006;312:2694–9.
5. Morales M, Theunissen JW, Kim CF, Kitagawa R, Kastan MB, Petrini JH. The Rad50S allele promotes ATM-dependent DNA damage responses and suppresses ATM deficiency: implications for the Mre11 complex as a DNA damage sensor. Genes Dev 2005;19:3043–54.
6. Bender CF, Sikes ML, Sullivan R, et al. Cancer predisposition and hematopoietic failure in Rad50(S/S) mice. Genes Dev 2002;16:2237–51.
7. Neale MJ, Pan J, Keeney S. Endonucleolytic processing of covalent protein-linked DNA double-strand breaks. Nature 2005;436:1053–7.
8. Stohr BA, Kreuzer KN. Repair of topoisomerase-mediated DNA damage in bacteriophage t4. Genetics 2001;158:19–28.
9. Connelly JC, Leach DR. Repair of DNA covalently linked to protein. Mol Cells 2004;13:307–16.
10. Kreuzer KN. Recombination-dependent DNA replication in phage T4. Trends Biochem Sci 2000;25:165–73.
11. Stracker TH, Carson CT, Weitzman MD. Adenovirus oncoproteins inactivate the Mre11-50-NBS1 DNA repair complex. Nature 2002;418:348–52.
12. Liu C, Pouliot JJ, Nash HA. Repair of topoisomerase I covalent complexes in the absence of the tyrosyl-DNA phosphodiesterase Tdp1. Proc Natl Acad Sci U S A 2002;99:14970–5.
13. Vance JR, Wilson TE. Yeast Tdp1 and Rad1-10 function as redundant pathways for repairing Top1 replicative damage. Proc Natl Acad Sci U S A 2002;99:13669–74.
14. Deng C, Brown JA, You D, Brown JM. Multiple endonucleases function to repair covalent topoisomerase I complexes in *Saccharomyces cerevisiae*. Genetics 2005;170:591–600.
15. Lacorazza HD, Yamada T, Liu Y, et al. The transcription factor MEF/ELF4 regulates the quiescence of primitive hematopoietic cells. Cancer Cell 2006;9:175–87.
16. Deng C, Zhang P, Harper JW, Elledge SJ, Leder P. Mice lacking p21CIP1/WAF1 undergo normal development, but are defective in G_1 checkpoint control. Cell 1995;82:675–84.
17. Kiyokawa H, Kineman RD, Manova-Todorova KO, et al. Enhanced growth of mice lacking the cyclin-dependent kinase inhibitor function of p27(Kip1). Cell 1996;85:721–32.
18. Barlow C, Hirotsune S, Paylor R, et al. Atm-deficient mice: a paradigm of ataxia telangiectasia. Cell 1996;86:159–71.
19. Hirao A, Cheung A, Duncan G, et al. Chk2 is a tumor suppressor that regulates apoptosis in both an ataxia telangiectasia mutated (ATM)-dependent and an ATM-independent manner. Molecular and cellular biology 2002;22:6521–32.
20. Spangrude GJ, Heimfeld S, Weissman IL. Purification and characterization of mouse hematopoietic stem cells. Science 1988;241:58–62.
21. Ikuta K, Weissman IL. Evidence that hematopoietic stem cells express mouse c-kit but do not depend on steel factor for their generation. Proc Natl Acad Sci U S A 1992;89:1502–6.
22. Okada S, Nakauchi H, Nagayoshi K, et al. Enrichment and characterization of murine hematopoietic stem cells that express c-kit molecule. Blood 1991;78:1706–12.
23. Bowie MB, Kent DG, Dykstra B, et al. Identification of a new intrinsically timed developmental checkpoint that reprograms key hematopoietic stem cell properties. Proc Natl Acad Sci U S A 2007;104:5878–82.
24. Sieburg HB, Cho RH, Dykstra B, Uchida N, Eaves CJ, Muller-Sieburg CE. The hematopoietic stem compartment consists of a limited number of discrete stem cell subsets. Blood 2006;107:2311–6.
25. Kondo M, Wagers AJ, Manz MG, et al. Biology of hematopoietic stem cells and progenitors: implications for clinical application. Ann Rev Immunol 2003;21:759–806.
26. Bowie MB, McKnight KD, Kent DG, McCaffrey L, Hoodless PA, Eaves CJ. Hematopoietic stem cells proliferate until after birth and show a reversible phase-specific engraftment defect. J Clin Invest 2006;116:2808–16.
27. Cheng T, Rodrigues N, Shen H, et al. Hematopoietic stem cell quiescence maintained by p21cip1/waf1. Science 2000;287:1804–8.
28. Cheng T, Rodrigues N, Dombkowski DSS, Scadden DT. Stem cell repopulation efficiency but not pool size is governed by p27kip1. Nature Medicine 2000;6:1235–40.
29. van Os R, Kamminga LM, Ausema A, et al. A Limited role for p21Cip1/Waf1 in maintaining normal hematopoietic stem cell functioning. Stem cells Dayton Ohio 2007;25:836–43.
30. Morrison C, Smith GCM, Stingl L, Jackson SP, Wagner EF, Wang Z-Q. Genetic interaction between PARP and DNA-PK in V(D)J recombination and tumorgenesis. Nat Genet 1997;17:479–83.
31. Nakayama K, Ishida N, Shirane M, et al. Mice lacking p27(Kip1) display increased body size, multiple organ hyperplasia, retinal dysplasia, and pituitary tumors. Cell 1996;85:707–20.
32. Fero ML, Rivkin M, Tasch M, et al. A syndrome of multiorgan hyperplasia with features of gigantism, tumorigenesis, and female sterility in p27(Kip1)-deficient mice. Cell 1996;85:733–44.
33. Hsiang YH, Hertzberg R, Hecht S, Liu LF. Camptothecin induces protein-linked DNA breaks via mammalian DNA topoisomerase I. J Biol Chem 1985;260:14873–8.
34. Chen GL, Yang L, Rowe TC, Halligan BD, Tewey KM, Liu LF. Nonintercalative antitumor drugs interfere with the breakage-reunion reaction of mammalian DNA topoisomerase II. J Biol Chem 1984;259:13560–6.
35. Tanabe K, Ikegami Y, Ishida R, Andoh T. Inhibition of topoisomerase II by antitumor agents bis(2,6-dioxopiperazine) derivatives. Cancer Res 1991;51:4903–8.
36. Pommier Y, Barcelo JM, Rao VA, et al. Repair of topoisomerase I-mediated DNA damage. Prog Nucleic Acid Res Mol Biol 2006;81:179–229.
37. Stracker TH, Morales M, Couto SS, Hussein H, Petrini JH. The carboxy terminus of NBS1 is required for induction of apoptosis by the MRE11 complex. Nature 2007;447:218–21.
38. Shaffer DR, Viale A, Ishiwata R, et al. Evidence for a p27 tumor suppressive function independent of its role regulating cell proliferation in the prostate. Proc Natl Acad Sci U S A 2005;102:210–5.
39. Carneiro C, Jiao MS, Hu M, et al. p27 deficiency desensitizes $Rb^{-/-}$ cells to signals that trigger apoptosis during pituitary tumor development. Oncogene 2003;22:361–9.
40. Yao JJ, Liu Y, Lacorazza HD, et al. Tumor promoting properties of the ETS protein MEF in ovarian cancer. Oncogene 2007;26:4032–7.